Journal of Materials Chemistry A

PAPER

View Article Online
View Journal | View Issue

Cite this: J. Mater. Chem. A, 2014, 2, 13527

Thermoelectric properties of Sn-doped p-type Cu_3SbSe_4: a compound with large effective mass and small band gap†

Tian-Ran Wei,‡[a] Heng Wang,‡[b] Zachary M. Gibbs,[b] Chao-Feng Wu,[a] G. Jeffrey Snyder[b] and Jing-Feng Li*[a]

Received 20th April 2014
Accepted 16th June 2014

DOI: 10.1039/c4ta01957a

www.rsc.org/MaterialsA

Cu_3SbSe_4-based compounds composed of earth-abundant elements have been found to exhibit good thermoelectric performance at medium temperatures. High zT values were achieved in previous studies, but further insight into the transport mechanism as well as some key material parameters is still needed. In this work, we studied the electrical and thermal transport properties of Sn-doped Cu_3SbSe_4 between 300 K and 673 K. It was found that the single parabolic band model explains the electrical transport very well. Experimentally, we determined the band gap to be around 0.29 eV. The density-of-state effective mass was found to be about 1.5 m_e for the doped samples. The transport properties suggested degeneracy splitting near the valence band maximum that was not captured by previous band structure calculations. The maximum $zT \sim 0.70$ was obtained at 673 K, and the optimized carrier density was $\sim 1.8 \times 10^{20}$ cm^{-3}, and the potential for further improvement of zT *via* material engineering is briefly discussed.

Introduction

Thermoelectric materials, which can realize the direct conversion between heat and electricity in the solid state, are expected to play a significant role in the field of clean energy development and utilization.[1] Developing materials with a high figure of merit, zT, defined as $zT = S^2T/\rho\kappa$ (S, T, ρ and κ are the Seebeck coefficient, absolute temperature, electrical resistivity and thermal conductivity, respectively), has been the main topic of research in thermoelectrics.[2–6] Recently, copper chalcogenides have received increasing attention as promising thermoelectric materials with a high zT, such as superionic Cu_2Se[7–9] with liquid-like phonon behaviour and layered oxyselenide BiCuSeO.[10–13] Other high-symmetry ternary or multinary copper chalcogenides composed of Cu–M (M is a chalcogen) tetrahedral bonds include chalcopyrite, tetrahedrite and famatinite, *etc.* Many of these compounds have also been found to be promising thermoelectrics, such as $CuGaTe_2$,[14,15] $CuInTe_2$,[16] $Cu_{2.1}Zn_{0.9}SnSe_4$,[17] $Cu_2ZnGeSe_4$[18] and Cu_3SbM_4 (M = Se, S),[19,20] even $Cu_{12}Sb_4S_{13}$ and $Cu_{12}As_4S_{13}$ right from their natural mineral form.[21,22] Among these compounds, Cu_3SbSe_4 is a p-type semiconductor with a small band gap. Previous investigations have been carried out focusing on adjusting the carrier density and forming solid solutions towards high zT.[23,24]

In spite of the knowledge that has already been obtained for Cu_3SbSe_4, the insight into the transport mechanism as well as some key material parameters that are essential for further optimization towards higher zT is still inadequate. In this work, we take a close look at the transport properties of p-type Cu_3SbSe_4. Our samples were prepared by mechanical alloying and spark plasma sintering. This simple method led to high quality samples with a homogeneous microstructure, nearly ideal doping efficiency and well behaved transport properties. This compound was found to be a semiconductor with a large effective mass of about 1.5 m_e (when doped) and a small band gap of $\sim$0.29 eV. The transport data also suggest a split of valence bands that was not revealed by previous calculations. These findings provide an in-depth understanding of the promising zT and the possible strategies for further material engineering.

Experimental

Samples with nominal compositions of $Cu_{2.95}Sb_{1-x}Sn_xSe_4$ (x = 0, 0.01, 0.02, 0.03, 0.04) were fabricated *via* mechanical alloying (MA) and spark plasma sintering (SPS). A Cu deficiency is chosen to compensate for Se volatilization and achieve the best performance, which was discussed in detail in a previous report.[25] A mixture of Cu, Sb, Sn and Se powders of high purity were milled in a stainless steel vessel on a planetary ball mill at 425 rpm for 10 hours protected by a mixed atmosphere of 95 vol% Ar and 5 vol% H_2 gases and were then milled in an

[a]State Key Laboratory of New Ceramics and Fine Processing, School of Materials Science and Engineering, Tsinghua University, Beijing 100084, China. E-mail: jingfeng@mail.tsinghua.edu.cn; Fax: +86-62771160; Tel: +86-10-62784845

[b]Materials Science, California Institute of Technology, Pasadena, CA 91125, USA

† Electronic supplementary information (ESI) available: Enlarged XRD patterns and calculation of the Lorenz number. See DOI: 10.1039/c4ta01957a

‡ Tian-Ran Wei and Heng Wang contributed equally to this work.

alcohol solution. The as-synthesized powders were sintered by SPS at 703 K for 5 min under a uniaxial pressure of 50 MPa into disk-shaped samples about 3 mm in thickness and about 93% or higher in relative density.

The phase structures were investigated by X-ray diffraction (XRD) with a D/max-RB diffractometer (Rigaku, Japan) using Cu Kα radiation. Scanning electron microscopy (SEM) images of the bulk materials were taken in the secondary electron detector (SE2) mode and the backscattering electron (BSE) mode by field emission scanning electron microscopy (FE-SEM, JSM-7001, JEOL, Japan). Electronic probe microscopic analysis (EPMA, JXA-8230, JEOL, Japan) was used to analyze the ratio and distribution of the elements on polished surface of bulk samples. Bar-shaped specimens were cut along the radial direction of a disk sample for measurements of the Seebeck coefficient (S) and the electrical resistivity (ρ) as a function of temperature using a Seebeck coefficient/electric resistance measuring system (ZEM-2, Ulvac-Riko, Japan). The Hall coefficient (R_H) at and above 300 K was measured under a reversible magnetic field by the van der Pauw technique using a Hall measurement system (8340DC, Toyo, Japan). The Hall carrier density (n_H) was calculated *via* $n_H = 1/(eR_H)$, and the Hall carrier mobility (μ_H) was obtained using the relationship, $\mu_H = R_H/\rho$. The thermal diffusivity (D) was measured in the thickness direction of a disk-shaped sample of ϕ 10 mm and about 1.5 mm in thickness using a laser flash diffusivity method (TC9000, Ulvac-Riko, Japan). The specific heat capacity (C_P) was measured using the Quantum Design physical property measurement system (PPMS) as well as the Netsch LFA 457 laser flash thermoanalysis system. The thermal conductivity (κ) was calculated by $\kappa = DC_pd$, where d is the density measured by the Archimedes method. Optical absorption edge measurements were carried out on the undoped sample using a Nicolet 6700 FTIR Spectrophotometer equipped with a Praying Mantis Diffuse Reflectance attachment (Harrick Scientific Instruments) at room temperature and up to 573 K. The scans were referenced to KBr standard samples. The optical gaps were obtained by extrapolating α, the absorption coefficient, to 0 as a function of $(h\nu)^n$, where $h\nu$ is the photon energy, and n is equal to 2 for direct gaps, 0.5 for indirect gaps.

Results and discussion

The XRD patterns of the samples subjected to SPS are shown in Fig. 1, which suggest single phase Cu_3SbSe_4 (PDF #85-0003) regardless of the Sn content. No peak shift even at high angles was found with the doping of Sn due to the small difference in ionic size[26] between Sn^{4+} and Sb^{5+} and the low doping level. The morphology of the fractured and polished surfaces of a representative sample of $Cu_{2.95}Sb_{0.98}Sn_{0.02}Se_4$ is shown in Fig. 2. The fractured surface exhibits well crystallized grains with an average grain size of ~2 μm. The back scattering electron (BSE) graph and EPMA mapping confirmed a homogeneous distribution of elements without the segregation of secondary phases.

Undoped Cu_3SbSe_4 is an intrinsic semiconductor with a carrier density in the order of 10^{18} cm^{-3}. Substituting Sn for Sb

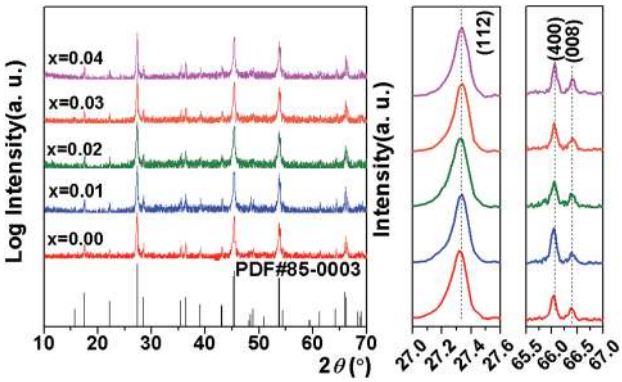

Fig. 1 XRD patterns of $Cu_{2.95}Sb_{1-x}Sn_xSe_4$. No peak shift due to Sn doping can be seen.

continuously increases the carrier density up to 2×10^{20} cm^{-3}. There has been debate on the specific valence number of Sb in Cu_3SbSe_4, both 5+ and 3 + have been suggested.[27–29] Nonetheless, with a simple argument that Sn has one less valence electron than Sb and is tetrahedrally bonded just as Sb in the structure, each Sn is expected to donate one free hole. This trend is well followed for the samples in the present study, as shown in Fig. 3: the measured Hall carrier density n_H at room temperature follows exactly the calculated result (solid line) based on the density of substitutional Sn atoms assuming each of them contribute one free hole, using the single parabolic band (SPB) model (which determines the Hall factor r_H that links n_H with the chemical carrier density n *via* $n_H = n/r_H$).

Fig. 4 shows the electrical resistivity (ρ) and Seebeck coefficient (S) as functions of temperature. All the samples showed p-type character. The undoped sample exhibited a nondegenerate

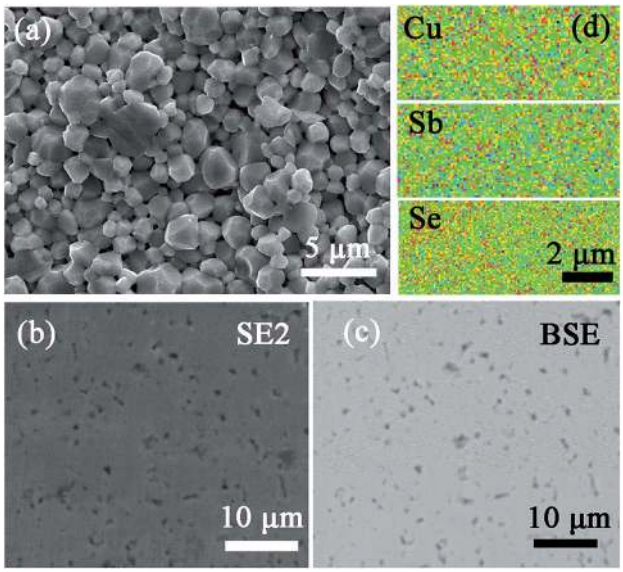

Fig. 2 Morphology and elemental distribution of bulk $Cu_{2.95}Sb_{0.98}Sn_{0.02}Se_4$: (a) SE2 image of a fractured surface; (b) SE2 image, (c) BSE image and (d) EPMA mapping of main elements of polished surface.

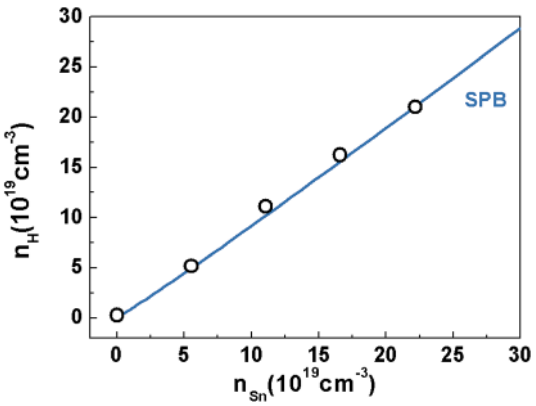

Fig. 3 Hall carrier density as a function of the dopant density at room temperature. The solid line was calculated by SPB assuming each Sn donates one free hole.

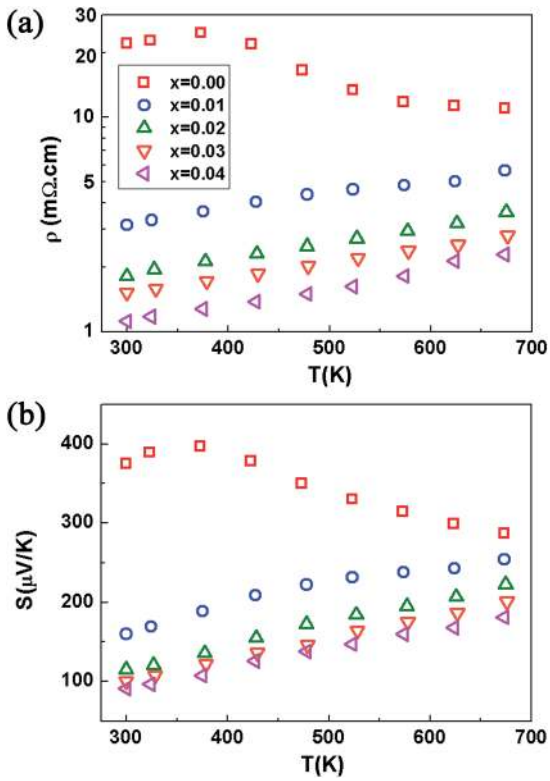

Fig. 4 (a) Electrical resistivity and (b) Seebeck coefficient as functions of temperature.

behaviour with a relatively large and decreasing Seebeck coefficient and resistivity with increasing temperature. From S of the undoped sample, the band gap E_g was estimated to be about 0.29 eV *via*[30]

$$E_g = 2eS_{max}T_{S_{max}}. \quad (1)$$

This estimate is consistent with the band gap measured by the optical absorption spectrum, which indicates a clear direct transition at 0.29 eV, as shown in Fig. 5. Previously, a similar band gap was reported by Berger *et al.* using the optical method.[31] We have also noticed that a much smaller gap of 0.13 eV was suggested by Nakanishi *et al.* by analyzing the temperature dependence of electrical resistivity and Hall coefficient, and 0.11 eV *via* the infrared transmission spectra.[32] A similar value was also obtained by Li *et al.* by fitting the electrical resistivity against temperature.[33] In fact, we found a similar activation energy of $\Delta E \sim 0.13$ eV in this study by fitting the linear relation, $\ln \rho - 1/T$, from the undoped sample. Further, our optical absorption measurements showed a very weak absorption above 0.12 eV, possibly corresponding to an indirect transition. However, we conclude that the activation energy of 0.12 eV is unlikely to be the primary band gap, because the large S values in undoped samples would not be achievable. In order to maintain a high Seebeck coefficient ($\sim$400 μV K^{-1} at $\sim$300 K), the chemical potential needs to be deep in the gap, while a small gap of 0.12 eV would inevitably induce significant minority carriers that compensate for the Seebeck value. As a result, the band gap is believed to be 0.29 eV corresponding to a direct transition, which is several orders of magnitude stronger than the supposed indirect transition. The activation energy of 0.12 eV is then speculated to be due to defect levels inside the band gap. Nakanishi *et al.* were not able to observe the much stronger direct transition because they used the optical transmission, which had already been saturated to zero throughput after the first indirect transition at 0.12 eV. A band gap around 0.3 eV is comparable with other good thermoelectrics, such as PbTe[34–36] or PbSe,[37–39] $Mg_2Si_{0.4}Sn_{0.6}$ (ref. 40) and ZrNiSn.[41] In addition, small band gaps usually mean less ionic character, making it easier for delocalized charge carriers that lead to high mobilities desirable for thermoelectrics. However, the disadvantage of a small band gap is the tendency of the excitation of minority carriers.

The measured Hall mobility, μ_H, of all samples decreased with increasing temperature [Fig. 6(a)]. Near room temperature, the $T^{-3/2}$ law is roughly obeyed by all samples, indicating the dominance of acoustic phonon scattering of carriers. Fig. 6(b) shows the measured n_H at different temperatures. For each doped sample, n_H remains constant near room temperature and

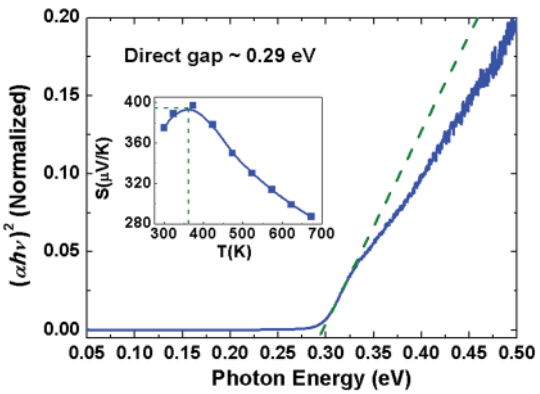

Fig. 5 Band gap by optical absorption edge measurements in undoped Cu_3SbSe_4.

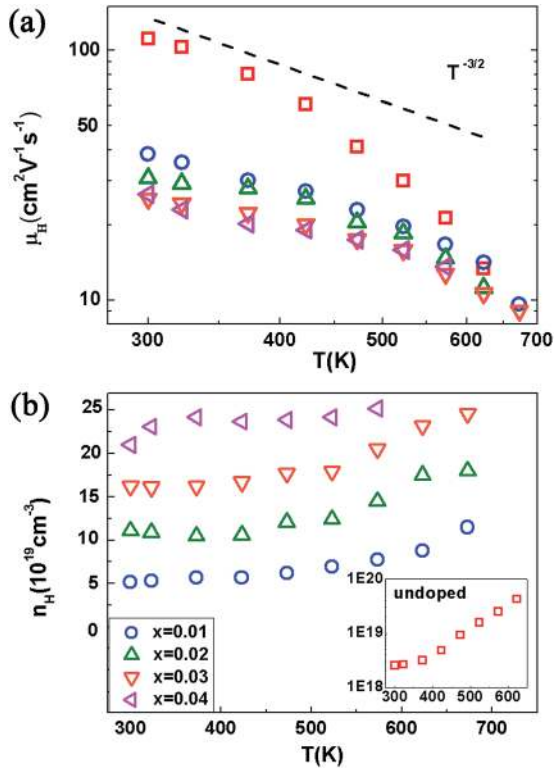

Fig. 6 (a) Hall mobility and (b) Hall carrier density as functions of temperature for $Cu_{2.95}Sb_{1-x}Sn_xSe_4$. The Hall carrier density of the undoped sample is depicted in the inset of (b).

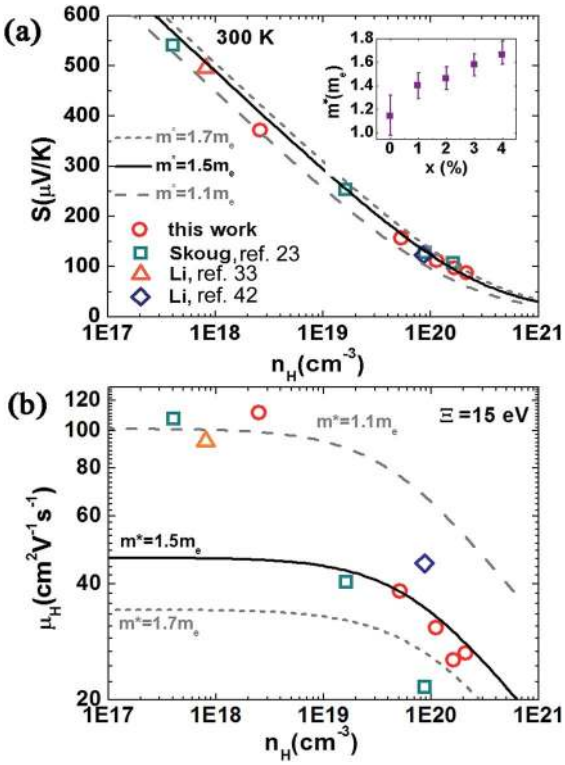

Fig. 7 Change in (a) Seebeck coefficient and (b) Hall mobility with the Hall carrier density at room temperature. The inset in (a) shows the effective mass for each sample determined from S and n_H.

above 500 K, it slowly increases with temperature. Considering a small and temperature-independent $E_g = 0.29$ eV in Cu_3SbSe_4, the apparent increase in n_H is likely due to bipolar excitation.

Fig. 7 shows the carrier density dependence of the Seebeck coefficient and Hall mobility at room temperature, together with the data previously reported for this system.[23,33,42] We found that the SPB model with acoustic phonon scattering assumption could well explain both properties. From the carrier density dependence of the Seebeck coefficient (the Pisarenko relation), it seems that all the measured S are consistent with a constant density-of-state (DOS) effective mass, $m^* = 1.5\ m_e$. However, a range of m^* values from 1.1 m_e to 1.7 m_e are acceptable. In fact, by calculating m^* for each individual sample, we found a clear increase when going from undoped to doped samples [inset of Fig. 7(a), error bars are estimated assuming 5% uncertainty in S measurement that is normally seen]. A large effective mass usually means less mobile carriers and a lower thermoelectric quality factor defined as:

$$B = \frac{2k_B{}^2\hbar}{3\pi}\frac{d{v_l}^2 N_V}{m_I^* \Xi^2 \kappa_L} T \qquad (2)$$

where v_l is the longitudinal speed of sound, d is the density, N_V is the degeneracy of band, m_I^* is the inertial effective mass, κ_L is the lattice thermal conductivity, and Ξ is the deformation potential coefficient.[43] However, in the case of Cu_3SbSe_4, the large m^* comes from three bands that are degenerate (suggested by calculation[29]) at the valence band maximum. As known in lead chalcogenides, a large effective mass from highly degenerate bands is favourable for high thermoelectric performance.[35]

The changing m^* with doping level is also indicated by the carrier density dependence of the Hall mobility μ_H. In the SPB model, μ_H of a system with a reduced chemical potential η can be expressed as:[43]

$$\mu_H = \frac{3\sqrt{\pi}}{8}\mu_0\frac{F_{-1/2}(\eta)}{F_0(\eta)} = \frac{\pi e\hbar^4 d{v_l}^2 N_V{}^{5/3}}{2\sqrt{2}m^{*5/2}(k_B T)^{3/2}\Xi^2}\frac{F_{-1/2}(\eta)}{F_0(\eta)} \qquad (3)$$

$$F_n(\eta) = \int_0^\infty \frac{x^n dx}{1+\exp(x-\eta)} \qquad (4)$$

where μ_0 is the nondegenerate limit of mobility governed by the acoustic phonon scattering process. We found that for doped samples, the SPB model provides a good fit with μ_0 determined to be 49 cm^2 V^{-1} s^{-1}. The measured mobility of the undoped sample on the other hand, is about twice as high as this value. We notice that all available reports[23,33,42] on undoped samples agree with our findings. Furthermore, for the sample studied in this work, this result is repeatable in at least two measurements from room temperature to 673 K. So the high mobilities are unlikely to be due to measurement error or non-equilibrium conditions. Using the SPB model, the difference can be well explained by the variation in effective mass considering m^* is 1.1 m_e for the undoped sample and 1.5 m_e for doped ones, as suggested in the inset of Fig. 7(a).

Previous band structure calculations for Cu_3SbSe_4 suggested a maximum of the valence band at the Γ point where three bands with different effective masses are degenerate.[29] The observed Pisarenko relation at 300 K, however, clearly implies a changing effective mass that cannot be explained by multiple degenerate bands. The observed transport properties instead suggest a split of at least two of these three bands near the maximum, possibly due to spin-orbit coupling, which was not considered in the reported calculation. Consequently, as the chemical potential moves deep into the valence bands with increasing carrier density, the secondary bands begin to play a more noticeable role in transport, leading to a larger m^* when the system is characterized with the SPB model.

While the observed Pisarenko relation and changing effective mass with increased doping level can be simply explained by the split of bands near the valence band maximum, the carrier density dependence of the mobility [seen in Fig. 7(b)] requires more complicated physics to completely understand it. Even with the band configuration, one would not expect the trend in Fig. 7(b) without allowing for inter-band scattering or additional scattering mechanisms associated with the increased density of dopants. Nonetheless, for the doped samples, which are of most interest to thermoelectrics, the SPB model with acoustic phonon scattering assumption still provides an effective way to understand the transport properties. With the reported v_l of 3643 m s^{-1},[27] and assuming $N_V = 3$,[29] the deformation potential coefficient Ξ, was found to be 15 ± 0.5 eV at 300 K. This value is smaller than those found in systems with a smaller effective mass, such as lead chalcogenides[44,45] and Bi_2Te_3,[46] whereas it is noticeably larger when compared with systems with a larger effective mass (>1 m_e for a single valley), such as La_3Te_4 (ref. 47), $Yb_{14}MnSb_{11}$ (ref. 48) and ZrNiSn.[49]

To determine the thermal conductivity of the samples, C_p was measured between 300 K and 673 K, and the values are shown in Fig. 8. We notice that the measured results from two different instruments, while consistent with each other, are considerably higher than the Dulong–Petit C_V. Above the Debye temperature (131 K by Berger *et al.*,[31] 60–80 K by Zhang *et al.*[27] and 65 K by Skoug *et al.*[50]), the C_P for solids is generally larger than C_V due to lattice expansion. While this qualitatively explains the linear increase in C_P with temperature, the difference at room temperature (20%) is much larger than one would expect. The difficulty in an accurate determination of C_P experimentally and thus the different values used by different studies is partially responsible for the difference in the reported zT values.

Fig. 9 shows the total thermal conductivity and the lattice thermal conductivity as functions of temperature. The electronic thermal conductivity κ_e was calculated by $\kappa_e = LT/\rho$, where the Lorenz number L, was calculated with the SPB model. The lattice thermal conductivity κ_L decreased with temperature following T^{-1} (dashed line), which indicates the dominance of phonon–phonon Umklapp scattering in phonon transport. Even in the undoped sample, κ_L decreased with T over the whole measurement range, and no obvious bipolar contribution was observed. Owing to the low percentage of Sn substitution and the small size difference between Sb and Sn, no difference in κ_L between doped and undoped samples was observed. The minimum lattice thermal conductivity for Cu_3SbSe_4, κ_{min}, was estimated using Cahill's formula[51] and was found be around 0.47 Wm^{-1} K^{-1} from 275 K to 700 K. Experimentally, κ_L at 673 K was around 1.1 Wm^{-1} K^{-1}, so a further reduction of κ_L is possible.

The figure of merit, zT, is shown as a function of temperature in Fig. 10(a). The maximum value ~0.70 was reached at 673 K in the sample with 2% Sn doping, and the corresponding Hall carrier density was $\sim 1.8 \times 10^{20}$ cm^{-3}. We further calculated zT

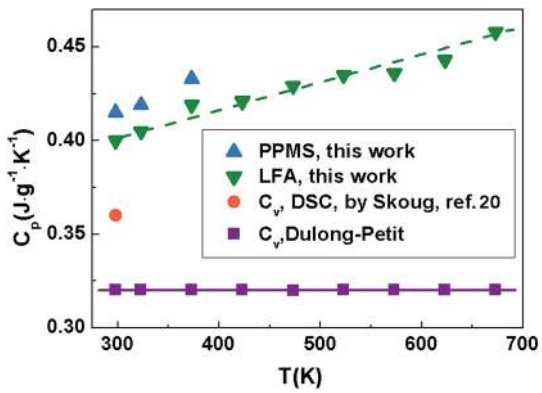

Fig. 8 Heat capacity as a function of temperature for undoped Cu_3SbSe_4. Skoug's result is 1.85 J cm^{-3} K^{-1} in ref. 20 and was converted to 0.36 J g^{-1} K^{-1} by assuming the relative density to be 90%.

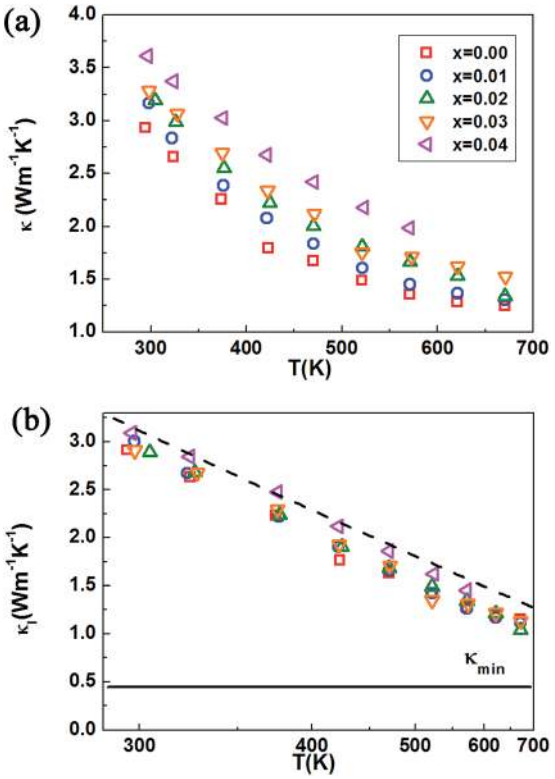

Fig. 9 (a) Total thermal conductivity and (b) lattice thermal conductivity as functions of temperature.

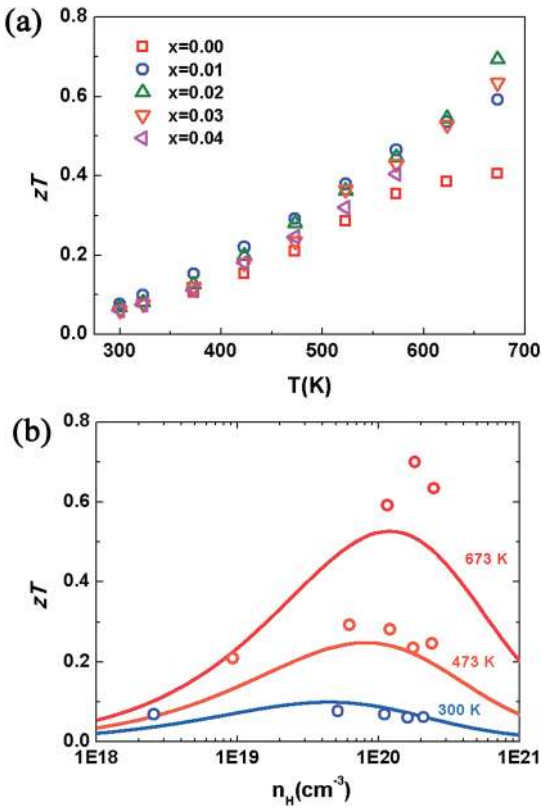

Fig. 10 zT as a function of (a) temperature and (b) Hall carrier density for Sn-doped Cu_3SbSe_4. Solid curves were calculated with SPB model using the parameters for doped samples determined at 300 K.

as a function of n_H from the SPB model using the parameters for doped samples determined at 300 K. The result is shown in Fig. 10(b). The optimal carrier density corresponding to the highest zT increased from ~4–5 × 10^{19} cm^{-3} at 300 K to ~1–2 × 10^{20} cm^{-3} at 673 K, as demonstrated experimentally and theoretically. According to the modeling, zT significantly higher than 0.7 is unlikely for Cu_3SbSe_4 just by tuning the carrier density. Two possible routes to a higher zT *via* material engineering are: first by tuning the position of individual valence bands, so they are better aligned at the maximum, and second by forming solid solutions which reduce κ_L. It should be noted that at high temperatures, Cu_3SbSe_4 has an inherent κ_L only twice as high as the theoretical minimum (comparable to the case of PbTe or PbSe where κ_L is around 0.7 Wm^{-1} K^{-1} and κ_{min} is around 0.4 Wm^{-1} K^{-1}) and that forming a solid solution will also decrease the carrier mobility. Therefore, forming solid solutions would likely increase zT but not significantly. Actually the zT value reported for $Cu_3SbSe_{4-x}S_x$ is 0.89: about a 20% increase over that of Cu_3SbSe_4 reported by the same group.[20,23]

Conclusions

Polycrystalline Cu_3SbSe_4 doped with Sn were fabricated with high phase purity and a precisely controlled carrier density by mechanical alloying and spark plasma sintering. The transport behaviour of this compound was explained by the single parabolic band (SPB) model. The Seebeck coefficients and mobilities at 300 K of the samples with different doping levels suggested a split of the bands at the valence band maximum, which according to previous calculations are triply degenerate. The transport data and optical band gap measurements suggested a direct band gap of ~0.29 eV, which is temperature independent. The thermal conductivity was governed by Umklapp phonon scattering, and a T^{-1} dependence was observed for all samples. The maximum zT value of ~0.70 was obtained at 673 K with 2% Sn (Hall carrier density 1.8 × 10^{20} cm^{-3}). The analyses and findings in this study would potentially help the understanding of transport properties in similar Cu-based ternary or multinary thermoelectric materials.

Acknowledgements

This work was supported by National Natural Science Foundation (no. 51172121) and the National Basic Research Program of China (Grant no. 2013CB632503) as well as 863 Program under Grant no. 2012AA051104. H. W., Z. M. G and G. J. S. acknowledge the support from the AFOSR MURI program in USA and the Molecular Materials Research Center (MMRC) at Caltech for optical measurement instruments.

Notes and references

1 L. E. Bell, *Science*, 2008, **321**, 1457–1461.
2 G. J. Snyder and E. S. Toberer, *Nat. Mater.*, 2008, **7**, 105–114.
3 J. R. Sootsman, D. Y. Chung and M. G. Kanatzidis, *Angew. Chem., Int. Ed.*, 2009, **48**, 8616–8639.
4 J.-F. Li, W.-S. Liu, L.-D. Zhao and M. Zhou, *NPG Asia Mater.*, 2010, **2**, 152–158.
5 J. Yang, H.-L. Yip and A. K.-Y. Jen, *Adv. Energy Mater.*, 2013, **3**, 549–565.
6 M. Zebarjadi, K. Esfarjani, M. S. Dresselhaus, Z. F. Ren and G. Chen, *Energy Environ. Sci.*, 2012, **5**, 5147–5162.
7 H. Liu, X. Shi, F. Xu, L. Zhang, W. Zhang, L. Chen, Q. Li, C. Uher, T. Day and G. J. Snyder, *Nat. Mater.*, 2012, **11**, 422–425.
8 H. Liu, X. Yuan, P. Lu, X. Shi, F. Xu, Y. He, Y. Tang, S. Bai, W. Zhang, L. Chen, Y. Lin, L. Shi, H. Lin, X. Gao, X. Zhang, H. Chi and C. Uher, *Adv. Mater.*, 2013, **25**, 6607–6612.
9 D. R. Brown, T. Day, K. A. Borup, S. Christensen, B. B. Iversen and G. J. Snyder, *APL Mater.*, 2013, **1**, 052107.
10 L. D. Zhao, D. Berardan, Y. L. Pei, C. Byl, L. Pinsard-Gaudart and N. Dragoe, *Appl. Phys. Lett.*, 2010, **97**, 092118.
11 J.-L. Lan, Y.-C. Liu, B. Zhan, Y.-H. Lin, B. Zhang, X. Yuan, W. Zhang, W. Xu and C.-W. Nan, *Adv. Mater.*, 2013, **25**, 5086–5090.
12 J. Sui, J. Li, J. He, Y.-L. Pei, D. Berardan, H. Wu, N. Dragoe, W. Cai and L.-D. Zhao, *Energy Environ. Sci.*, 2013, **6**, 2916–2920.
13 F. Li, J.-F. Li, L.-D. Zhao, K. Xiang, Y. Liu, B.-P. Zhang, Y.-H. Lin, C.-W. Nan and H.-M. Zhu, *Energy Environ. Sci.*, 2012, **5**, 7188–7195.
14 J. Cui, Y. Li, Z. Du, Q. Meng and H. Zhou, *J. Mater. Chem. A*, 2013, **1**, 677–683.

15 J. Zhang, X. Qin, D. Li, H. Xin, C. Song, L. Li, X. Zhu, Z. Wang, G. Guo and L. Wang, *J. Mater. Chem. A*, 2014, **2**, 2891–2895.
16 R. Liu, L. Xi, H. Liu, X. Shi, W. Zhang and L. Chen, *Chem. Commun.*, 2012, **48**, 3818–3820.
17 M.-L. Liu, F.-Q. Huang, L.-D. Chen and I. W. Chen, *Appl. Phys. Lett.*, 2009, **94**, 202103.
18 W. G. Zeier, Y. Pei, G. Pomrehn, T. Day, N. Heinz, C. P. Heinrich, G. J. Snyder and W. Tremel, *J. Am. Chem. Soc.*, 2013, **135**, 726–732.
19 D. Li, R. Li, X.-Y. Qin, J. Zhang, C.-J. Song, L. Wang and H.-X. Xin, *CrystEngComm*, 2013, **15**, 7166–7170.
20 E. J. Skoug, J. D. Cain and D. T. Morelli, *Appl. Phys. Lett.*, 2011, **98**, 261911.
21 X. Lu, D. T. Morelli, Y. Xia, F. Zhou, V. Ozolins, H. Chi, X. Zhou and C. Uher, *Adv. Energy Mater.*, 2013, **3**, 342–348.
22 X. Lu and D. T. Morelli, *Phys. Chem. Chem. Phys.*, 2013, **15**, 5762–5766.
23 E. J. Skoug, J. D. Cain, P. Majsztrik, M. Kirkham, E. Lara-Curzio and D. T. Morelli, *Sci. Adv. Mater.*, 2011, **3**, 602–606.
24 C. Yang, F. Huang, L. Wu and K. Xu, *J. Phys. D: Appl. Phys.*, 2011, **44**, 295404.
25 T.-R. Wei, F. Li and J.-F. Li, *J. Electron. Mater.*, 2014, **43**, 2229–2238.
26 R. D. Shannon, *Acta Crystallogr., Sect. A: Cryst. Phys., Diffr., Theor. Gen. Crystallogr.*, 1976, **32**, 751–767.
27 Y. Zhang, E. Skoug, J. Cain, V. Ozoliņš, D. Morelli and C. Wolverton, *Phys. Rev. B: Condens. Matter Mater. Phys.*, 2012, **85**, 054306.
28 E. J. Skoug and D. T. Morelli, *Phys. Rev. Lett.*, 2011, **107**, 235901.
29 D. Do, V. Ozolins, S. D. Mahanti, M.-S. Lee, Y. Zhang and C. Wolverton, *J. Phys.: Condens. Matter*, 2012, **24**, 415502.
30 H. J. Goldsmid and J. W. Sharp, *J. Electron. Mater.*, 1999, **28**, 869–872.
31 L. I. Berger and V. D. Prochukhan, *Ternary Diamond-Like Semiconductors*, Consultants Bureau, New York, 1969.
32 H. Nakanishi, S. Endo and T. Irie, *Jpn. J. Appl. Phys.*, 1969, **8**, 443–449.
33 X. Y. Li, D. Li, H. X. Xin, J. Zhang, C. J. Song and X. Y. Qin, *J. Alloys Compd.*, 2013, **561**, 105–108.
34 Y. I. Ravich, B. A. Efimova and I. A. Smirnov, *Semiconducting Lead Chalcogenides*, Plenum, New York, 1970.
35 Y. Pei, X. Shi, A. D. LaLonde, H. Wang, L. Chen and G. J. Snyder, *Nature*, 2011, **473**, 66–69.
36 Z. M. Gibbs, A. D. LaLonde and G. J. Snyder, *New J. Phys.*, 2013, **15**, 075020.
37 H. Wang, Z. M. Gibbs, Y. Takagiwa and G. J. Snyder, *Energy Environ. Sci.*, 2014, **7**, 804–811.
38 Z. M. Gibbs, H. Kim, H. Wang, R. L. White, F. Drymiotis, M. Kaviany and G. Jeffrey Snyder, *Appl. Phys. Lett.*, 2013, **103**, 262109.
39 H. Wang, Y. Pei, A. D. LaLonde and G. J. Snyder, *Adv. Mater.*, 2011, **23**, 1366–1370.
40 W. Liu, X. Tan, K. Yin, H. Liu, X. Tang, J. Shi, Q. Zhang and C. Uher, *Phys. Rev. Lett.*, 2012, **108**, 166601.
41 Q. Shen, L. Chen, T. Goto, T. Hirai, J. Yang, G. P. Meisner and C. Uher, *Appl. Phys. Lett.*, 2001, **79**, 4165.
42 D. Li, R. Li, X.-Y. Qin, C.-J. Song, H.-X. Xin, L. Wang, J. Zhang, G.-L. Guo, T.-H. Zou, Y.-F. Liu and X.-G. Zhu, *Dalton Trans.*, 2014, **43**, 1888–1896.
43 H. Wang, Y. Pei, A. D. LaLonde and G. J. Snyder, in *Thermoelectric Nanomaterials: Materials Design and Applications*, ed. K. Koumoto and T. Mori, Springer, Heidelberg, 2013, pp. 3–32.
44 H. Wang, Y. Pei, A. D. LaLonde and G. J. Snyder, *Proc. Natl. Acad. Sci. U. S. A.*, 2012, **109**, 9705–9709.
45 H. Wang, E. Schechtel, Y. Pei and G. J. Snyder, *Adv. Energy Mater.*, 2013, **3**, 488–495.
46 B.-L. Huang and M. Kaviany, *Phys. Rev. B: Condens. Matter Mater. Phys.*, 2008, **77**, 125209.
47 A. F. May, J.-P. Fleurial and G. J. Snyder, *Phys. Rev. B: Condens. Matter Mater. Phys.*, 2008, **78**, 125205.
48 E. S. Toberer, C. A. Cox, S. R. Brown, T. Ikeda, A. F. May, S. M. Kauzlarich and G. J. Snyder, *Adv. Funct. Mater.*, 2008, **18**, 2795–2800.
49 H. Xie, H. Wang, Y. Pei, C. Fu, X. Liu, G. J. Snyder, X. Zhao and T. Zhu, *Adv. Funct. Mater.*, 2013, **23**, 5123–5130.
50 E. J. Skoug, J. D. Cain, D. T. Morelli, M. Kirkham, P. Majsztrik and E. Lara-Curzio, *J. Appl. Phys.*, 2011, **110**, 023501.
51 D. G. Cahill, S. K. Watson and R. O. Pohl, *Phys. Rev. B: Condens. Matter Mater. Phys.*, 1992, **46**, 6131–6140.